Colorimetric sensing of dopamine in beef meat using copper sulfide encapsulated within bovine serum albumin functionalized with copper phosphate (CuS-BSA-Cu3(PO4)2) nanoparticles

Abir Swaidan, Alexandre Barras, Ahmed Addad, Jean-Francois Tahon, Joumana Toufaily, Tayssir Hamieh, Sabine Szunerits, Rabah Boukherroub

Colorimetric sensing of dopamine in beef meat using copper sulfide encapsulated within bovine serum albumin functionalized with copper phosphate (CuS-BSA-$Cu_3(PO_4)_2$) nanoparticles

Abir Swaidan,[a,b] Alexandre Barras,[a] Ahmed Addad,[c] Jean-Francois Tahon,[c] Joumana Toufaily,[b] Tayssir Hamieh,[b] Sabine Szunerits,[a] and Rabah Boukherroub[a*]

[a]*Univ. Lille, CNRS, Centrale Lille, Univ. Polytechnique Hauts-de-France, UMR 8520 - IEMN, F-59000 Lille, France*

[b]*Univ. Libanaise, LEADDER, Laboratoire des études appliquées au développement durable et énergie renouvelable, Hadath, Liban*

[c]*Univ. Lille, CNRS, UMR 8207 – UMET, F-59000 Lille, France*

*To whom correspondence should be addressed: Rabah Boukherroub, e-mail: rabah.boukherroub@univ-lille.fr; Tel: +333 62 53 17 24

Abstract

A novel nanosensor with peroxidase enzyme-mimetic activity, based on CuS-BSA-$Cu_3(PO_4)_2$ nanoparticles, was developed. CuS-BSA nanoparticles were first synthesized using a facile bio-mineralization assay. Conjugation of $Cu_3(PO_4)_2$ with CuS-BSA generates CuS-BSA-$Cu_3(PO_4)_2$ nanoparticles (NPs) of 10 nm in size with high catalytic activity against a peroxidase substrate, 3,3′,5,5′-tetramethylbenzidine (TMB). The catalytic action was based on a remarkable color change from colorless TMB into blue oxidized product (oxTMB) with absorption maximum at 654 nm. The enzyme-mimetic activity of CuS-BSA-$Cu_3(PO_4)_2$ nanoparticles was believed to occur through hydroxyl radical ($HO^{\bullet}$) generation in presence of H_2O_2, which was inhibited upon addition of dopamine. Increasing concentrations of dopamine induced a gradual decrease of the nanoparticles' catalytic activity. The developed colorimetric sensor displayed a limit of detection of 0.13 µM for dopamine over 0.05-100 µM linear range and high specificity. The performance of the nanosensor for sensing dopamine in beef meat and blood samples was evaluated and proved to be promising for diagnostic applications without the requirement of complex and expensive instrumentation.

Keywords: *CuS-BSA-$Cu_3(PO_4)_2$; nanozymes; colorimetric; detection; dopamine; beef meat.*

1. Introduction

Dopamine (DA) is a biogenic amine that forms as a result of amino acid decarboxylation, and is a proven anti-oxidant against the damaging effect of free radicals [1]. DA is also considered as an essential catecholamine neurotransmitter in the central nervous system, and an important contributor in human metabolism. The dopamine hydrochloride salt can be used in the treatment of severe diseases like heart attack, kidney failure, as well blood infections caused by bacteria [2]. However, abnormal release of dopamine in the human body can cause Alzheimer, Huntington, Parkinson, Schizophrenia and many neuronal diseases [3, 4].

In addition, DA is used in animal feed to lower the amount of fat in animal species and help build muscles [5, 6]. However, DA residues are susceptible to accumulate in tissues, which represents a major hazard to animal species even if they are exposed to a low level of DA. Therefore, the detection of DA with high accuracy represents an indispensable need to achieve early disease diagnosis. Due to the significant importance of this molecule, various methods such as high-performance liquid chromatography (HPLC) [7], electrophoresis [8], chemiluminescence [9], capillary electrophoresis [10], and particularly electrochemical means [11-13] have been used for the quantification of DA concentration in different samples.

Recently, optical spectroscopic methods based on colorimetric assays gained much attention for DA sensing due to their simplicity and high sensitivity. Indeed, methods for DA detection should be highly sensitive due to the low amount of this molecule in physiological media [14]. Additionally, DA coexists with ascorbic acid (AA) and uric acid (UA) in physiological samples [15, 16], which hampers the quantification of dopamine due to the potential interference with these molecules. Additionally, the presence of these molecules might influence the specificity of detection.

Since the successful utilization of nanomaterials as new members of artificial enzymes, an enormous array of enzyme-mimetics or nanozymes [17] have been developed as novel colorimetric detection schemes for sensing of a wide range of chemical and biological molecules [18]. In this context, nanozymes occupy a central place and have been extensively investigated in the field of sensing and proved to be promising alternatives to analytical sensing devices due to their exceptional properties [18, 19]. Shiyun and colleagues reported a colorimetric assay for DA determination by taking advantage of gold NPs aggregation mediated by Cu^{2+} ions [20]. Wang *et al.* investigated a composite material of reduced graphene oxide (rGO) conjugated with $NiCo_2S_4$ for colorimetric DA sensing [21]; many other reported materials have been utilized for DA sensing using colorimetric assays [3, 4, 22-24]. In these circumstances, colorimetric sensing provided highly sensitive and selective monitoring of biological molecules, in addition to fast time response that can record concentration changes which occur at a second time scale.

Tremendous attention has been devoted to Cu-based nanomaterials such as copper oxide (CuO), Zn-doped CuO, copper-containing metal organic frameworks (Cu-MOFs) and copper phosphate $Cu_3(PO_4)_2$, etc. [25-28] for sensing and catalysis-related applications [29]. In particular, copper sulfide (CuS) based nanomaterials have shown to be promising nanozymes for glucose, cholesterol, heavy metal ions, and uric acid sensing [30-34], due to their enzymatic-like behavior for the catalyzed oxidation of peroxidase substrates in presence of H_2O_2. A CuS-based sensor has been reported previously by Tarasankar and co-workers in combination with rGO [24] for sensing dopamine. However, the nanocomposite displayed low sensitivity and selectivity.

Herein, we report on a colorimetric dopamine sensor based on the intrinsic peroxidase mimetic activity of CuS-BSA-$Cu_3(PO_4)_2$ nanoparticles, synthesized through CuS NPs conjugation with copper phosphate ($Cu_3(PO_4)_2$) using bovine serum albumin (BSA) as a linker and stabilizer.

Coupling of $Cu_3(PO_4)_2$ to CuS-BSA nanoparticles not only enhanced their effective enzyme-like catalytic activity over natural enzymes and other reported nanomaterials, but also produced particles with ultrasmall size. The colorimetric sensor follows a typical Michaelis-Menten model with high affinity to H_2O_2 and TMB. On the basis of this result, we demonstrated a rapid sensing platform of dopamine (DA), in which an immense reduction of $HO^{\bullet}$ radical generation and an inhibition of the catalytic oxidization action towards TMB have been achieved in the presence of DA. The technique was highly sensitive and selective and was applied successfully for DA sensing in meat and blood samples.

2. Experimental section

2.1. Materials and methods

Copper(II) sulfate pentahydrate ($CuSO_4.5H_2O$, ≥98.0%), copper(II) acetate ($Cu(Ac)_2$, 98.0%), bovine serum albumin (BSA, ≥96.0%), sodium acetate anhydrous (CH_3COONa, ≥99.0%), sodium hydroxide pellets (NaOH, ≥97.0%), sodium sulfide hydrate ($Na_2S.\times H_2O$, ≥97.0%), 3,3',5,5'-tetramethylbenzidine (TMB, ≥95.0%), dopamine hydrochloride ($C_8H_{11}NO_2\cdot HCl$), β-Lactose ($C_{12}H_{22}O_{11}$, ≥99.0%), L-Glutathione reduced ($C_{10}H_{17}N_3O_6S$, ≥98%), uric acid ($C_5H_4N_4O_3$, ≥99.0%), L-Ascorbic acid ($C_6H_8O_6$, ≥99.0%), D(-)-Fructose ($C_6H_{12}O_6$, ≥99.0%), α-D-Glucose ($C_6H_{12}O_6$, 96.0%), cholesterol ($C_{27}H_{46}O$, ≥99.0%), phosphate buffered saline pellets (PBS), zinc chloride ($ZnCl_2$, 99.9 %) and terephthalic acid (C_6H_4-1,4-$(CO_2H)_2$, 98.0%) were purchased from Sigma-Aldrich. Glacial acetic acid (99.0%), ethanol (95% v/v), dimethyl sulfoxide (DMSO, ≥99.9%), hydrochloric acid (HCl, ~37%), *t*-butyl alcohol (TBA, 99%) and hydrogen peroxide (H_2O_2, 30 wt.%) were purchased from Fisher Scientific.

Milli-Q (MQ) water was used throughout the entire study. Beef meat was obtained from a local supermarket (Lille, France), and human serum samples were obtained from a male volunteer at CHU Lille, France.

2.2. Preparation of CuS-BSA-$Cu_3(PO_4)_2$ enzyme-mimetic nanoparticles

The synthetic route of CuS-BSA-$Cu_3(PO_4)_2$ comprises two sequential steps.

2.2.1. Synthesis of CuS-BSA nanoparticles

In brief, 63 mg of BSA lyophilized powder and 9 mL of Milli-Q water were placed in a 50 mL round bottom flask. To this solution, 162 mg of copper acetate [$Cu(Ac)_2$] and 0.5 mL of NaOH (2.0 M) were sequentially added under continuous magnetic stirring to ensure homogeneous dispersion. Then 117 mg of $Na_2S.xH_2O$ were added and the reaction mixture was heated in an oil bath at 90 °C for 5 h. The formed CuS-BSA product was purified by using a 12000-14000 Da molecular mass cutoff dialysis membrane against Milli-Q water for 24 h.

2.2.2. Synthesis of CuS-BSA-$Cu_3(PO_4)_2$ nanoparticles

10 mg of the as-synthesized CuS-BSA were mixed with 0.1 mL aqueous solution of $CuSO_4.5H_2O$ (80 mM) in 9.9 mL PBS (0.01 M, pH 7.4), and kept at 4 °C for 72 h under magnetic agitation. The obtained CuS-BSA-$Cu_3(PO_4)_2$ product was purified by dialysis using a 12000-14000 Da molecular mass cutoff dialysis membrane in Milli-Q water for 24 h, after which it is lyophilized to obtain a green powder.

2.2.3. Synthesis of $Cu_3(PO_4)_2$-BSA

$Cu_3(PO_4)_2$-BSA NPs were prepared as follows: In brief, 0.1 mL aqueous solution of $CuSO_4.5H_2O$ (80 mM) were mixed with 10 mg BSA in 9.9 mL PBS (0.01 M, pH 7.4) and incubated at 4 °C for

72 h. The obtained $Cu_3(PO_4)_2$-BSA was then purified by centrifugation (8500 rpm for 15 min at 4 °C) and washing with Milli-Q water.

2.3. Enzyme-mimetic activity of CuS-BSA-$Cu_3(PO_4)_2$ nanoparticles

The enzyme-like catalytic action of CuS-BSA-$Cu_3(PO_4)_2$ towards the oxidation of a peroxidase chromogenic substrate, 3,3′,5,5′-tetramethylbenzidine (TMB), was assessed as following. In a typical procedure, the reaction was performed by mixing 0.1 mL of CuS-BSA-$Cu_3(PO_4)_2$ (1 mg/mL) as a catalyst, 0.1 mL of H_2O_2 (10 mM) and 10 µL TMB (30 mM in DMSO) in 0.79 mL of acetate buffer (0.1 M, pH 4) for 20 min at room temperature (RT). UV-vis absorption spectroscopy (380-800 nm range) was used to monitor the absorbance variation at 654 nm, which corresponds to the oxidized product of TMB (oxTMB).

The influence of various parameters such as CuS-BSA-$Cu_3(PO_4)_2$ concentration (0-0.15 mg/mL), TMB concentration (0.01-0.35 mM), incubation time (0-30 min), temperature (25-70 °C), and pH (3.6-10) on the catalytic reaction were assessed to determine the optimal conditions.

Control experiments were run in the absence of catalyst or H_2O_2, and with both CuS-BSA-$Cu_3(PO_4)_2$ catalyst and H_2O_2 for comparison.

TMB oxidation was also examined before and after coupling CuS-BSA with $Cu_3(PO_4)_2$ to study their influence on the catalytic properties of the nanozyme.

2.4. Colorimetric determination of hydrogen peroxide (H_2O_2)

The enzyme-mimetic activity of CuS-BSA-$Cu_3(PO_4)_2$ was evaluated for H_2O_2 quantification in an acidic environment by mixing different H_2O_2 concentrations (0-1.2 mM) with 0.1 mg/mL CuS-BSA-$Cu_3(PO_4)_2$ and 0.3 mM TMB in 1 mL of acetate buffer (0.1 M, pH 4) for 20 min at RT. The

absorption maximum at 654 nm was monitored, enabling to generate a linear calibration plot for H_2O_2 for the limit of detection (LOD) determination using Eq. 1:

$$LOD = 3\sigma/a \qquad (1)$$

Where σ represents the baseline standard deviation, and a is the slope of the linear calibration curve.

2.5. Michaelis-Menten model of CuS-BSA-$Cu_3(PO_4)_2$ towards the determination of K_m and V_{max}

The rate of the CuS-BSA-$Cu_3(PO_4)_2$-catalyzed reaction and affinity towards a targeted substrate were evaluated using the Michaelis-Menten mathematical model. By choosing two different substrates, TMB and H_2O_2, the catalytic reaction rate which is defined as V_{max}, and the affinity which is evaluated from a Michaelis-Menten constant termed "K_m", can be determined from a Lineweaver-Burk plot represented in Eq. 2:

$$\frac{1}{v} = \frac{1}{[S]} \times \frac{K_m}{V_{max}} + \frac{1}{V_{max}} \qquad (2)$$

Where v is the initial reaction rate, K_m represents the Michaelis–Menten constant, V_{max} corresponds to the maximum reaction rate, and [S] is the substrate concentration.

Various experiments were conducted to evaluate the reaction kinetic parameters by monitoring the absorption maximum at 654 nm through eliciting H_2O_2 as a substrate at variable concentrations and fixed TMB concentration or *vice versa*.

Kinetic measurements were recorded for the reaction of varying H_2O_2 concentrations (0-1.2 mM) with 0.3 mM TMB and 0.1 mg/mL (CuS-BSA-$Cu_3(PO_4)_2$) in 1 mL acetate buffer (0.1 M, pH 4). Similarly, kinetic experiments were determined by mixing TMB substrate (0.01-0.35 mM) with 1

mM H_2O_2 and 0.1 mg/mL (CuS-BSA-$Cu_3(PO_4)_2$) in 1 mL acetate buffer (0.1 M, pH 4). All the kinetic measurements were carried out in a time-scan mode.

2.6. Catalytic mechanism of CuS-BSA-$Cu_3(PO_4)_2$ towards the generation of hydroxyl ($HO^{\bullet}$) radicals

It is generally approved that oxidation of TMB proceeds through the generation of $HO^{\bullet}$ radicals from H_2O_2 [35]. To confirm this hypothesis, we investigated the fluorescent probe experiment using terephthalic acid (TA). Briefly, 10 µL of terephthalic acid (TA, 20 mM dissolved in DMSO) was separately mixed with 100 µL of (a) H_2O_2 (10 mM), (b) CuS-BSA-$Cu_3(PO_4)_2$ (1 mg/mL), (c) DA (2 mM), (d) DA (2 mM) + H_2O_2 (10 mM), (e) DA (2 mM) + CuS-BSA-$Cu_3(PO_4)_2$ (1 mg/mL), (f) DA (2 mM) + CuS-BSA-$Cu_3(PO_4)_2$ (1 mg/mL) + H_2O_2 (10 mM), (g) H_2O_2 (10 mM) + CuS-BSA-$Cu_3(PO_4)_2$ (1 mg/mL) for 20 min at RT, and the volume was adjusted to 1 mL by acetate buffer (0.1 M, pH 4). Fluorescence emission was then collected within the 393-530 nm range using a fluorescence spectrophotometer at excitation wavelength of 318 nm.

Furthermore, we conducted additional experiments in the presence of ROS scavengers, such as *t*-butyl alcohol (TBA), which readily known to quench $HO^{\bullet}$ radicals. Thus, to a mixture of CuS-BSA-$Cu_3(PO_4)_2$ (0.1 mg/mL), H_2O_2 (1 mM) and TMB (0.3 mM), 0.4 mM of TBA was added in acetate buffer (0.1 M, pH 4) for 20 min at RT. Absorption spectra at 654 nm were then recorded to follow the changes of TMB oxidation by $HO^{\bullet}$ radicals.

2.7. Colorimetric assay for sensing dopamine (DA)

Similarly, to further widen the scope of the sensor, we have demonstrated the direct sensing of DA using the optimized conditions. DA detection was carried out by adding freshly prepared dopamine.HCl aqueous solutions of different concentrations (0-0.5 mM) to a mixture of CuS-

BSA-$Cu_3(PO_4)_2$ (0.1 mg/mL), TMB (0.3 mM), and H_2O_2 (1 mM) in acetate buffer solution (0.1 M, pH 4) of total volume of 1 mL. After incubation for 20 min at RT, the sequential change in the absorption (A_{654nm}) of oxTMB at variable DA concentrations was recorded and the LOD was calculated using Eq. 1.

2.8. Selectivity and reproducibility of CuS-BSA-$Cu_3(PO_4)_2$ nanosensor

The selectivity of CuS-BSA-$Cu_3(PO_4)_2$ towards DA sensing was assessed using 0.3 mM (same as optimum DA concentration) of lactose, glutathione, uric acid, cholesterol, glucose, fructose, ascorbic acid or 0.6 mM (2× higher than DA concentration) in presence of TMB (0.3 mM), H_2O_2 (1 mM) and CuS-BSA-$Cu_3(PO_4)_2$ (0.1 mg/mL) in 1 mL acetate buffer (0.1 M, pH 4) for 20 min at RT.

The reproducibility of the nanosensor was also examined under the optimum reaction parameters for 4 successive cycles. Before each cycle, the mixture was centrifuged at 13500 rpm for 3 min to collect the catalyst which was then washed with MQ-water to remove any traces of H_2O_2 or oxTMB, to be ready for the next cycle.

2.9. DA sensing in meat and blood samples

To achieve an excellent colorimetric practicality, selectivity is highly crucial in real samples. Thus, DA sensing was evaluated in meat samples collected from a local supermarket (Lille, France) and prepared according to our previous procedure [36]. Typically, ~4.0 g of beef meat was cut into small pieces and grinded well using a mortar and pestle, after which 10 mL of PBS buffer solution (0.1 M, pH 7.4) was added, followed by 10 mL of $ZnCl_2$ solution (1 M) to induce protein precipitation. The mixture was moderately agitated for 20 min at 100 rpm, centrifuged for 15 min

at 4 °C with a speed of 4000 rpm, and filtered 2× using a Minisart filter (0.2 µm pore size). The obtained supernatant was then used for the detection of dopamine.

In brief, 20 µL of meat solution were mixed with 100 µL of CuS-BSA-$Cu_3(PO_4)_2$ (1 mg/mL), 100 µL of H_2O_2 (10 mM), and 10 µL of TMB (30 mM) in 1 mL acetate buffer (0.1 M, pH 4) for 20 min at RT. The amount of dopamine in meat samples was assessed by recording the absorbance maximum at 654 nm.

High performance liquid chromatography (HPLC) analysis was used to confirm the results for determining the concentration of DA in meat samples.

The validity of the developed nanosensor was extended by analyzing dopamine content in human blood samples. Serum samples were taken from a male volunteer at CHU Lille hospital, France. Samples were centrifuged for 5 min at 13,500 rpm, and the serum was collected and diluted 1000 times to make sure that the DA content is within our established calibration plot. 1 µL of the diluted serum solution was then mixed with DA at various concentrations (5, 10, 15, 50 µM). CuS-BSA-$Cu_3(PO_4)_2$ (0.1 mg/mL), H_2O_2 (1 mM), and TMB (0.3 mM) were added successively to the reaction mixture, and the volume was adjusted to 1 mL using acetate buffer (0.1 M, pH 4). After 20 min incubation at RT, the absorbance of oxTMB at 654 nm was monitored using UV-vis spectrophotometry.

3. Results and discussion

3.1. Sample characterization

CuS-BSA-$Cu_3(PO_4)_2$ nanoparticles were synthesized *via* a bio-mineralization process and characterized using different techniques. As illustrated from the dynamic scattering analysis (DLS) in **Figures S1 and S2**, conjugation of CuS-BSA with $Cu_3(PO_4)_2$ induces a noticeable slight

increase in both the negative surface charge and diameter. Indeed, the surface charge of CuS-BSA changed from -26 ± 2.8 mV to -29 ± 2.6 mV upon incorporation of $Cu_3(PO_4)_2$, while the diameter increased from 54 nm up to 143 nm.

The successful synthesis of the nanoparticles and the presence of diverse functional groups were additionally confirmed by FTIR analysis. Compared to the CuS-BSA FTIR spectrum, **Figure S3** reveals the existence of characteristic vibration peaks at 1046 and 981 cm^{-1} ascribed to asymmetrical P=O and symmetrical P-O stretchings, respectively [37, 38] in the CuS-BSA-$Cu_3(PO_4)_2$ FTIR spectrum. The characteristic peak at 1115 cm^{-1} corresponds to CuS [39], while the peaks at 3433, 1652, 1543, 1381 cm^{-1} are ascribed to O-H, C=O (amide I), N-H (amide II), and C-H stretching modes in BSA, respectively [40].

To investigate the optical properties of CuS-BSA-$Cu_3(PO_4)_2$, the UV-vis-NIR absorption spectra were recorded in the 200-1000 nm range. The obtained results **(Fig. S4)** reveal that CuS-BSA-$Cu_3(PO_4)_2$ and CuS-BSA both exhibit a broad absorption band in the visible with a concomitant band in the NIR range. All these results confirm the successful synthesis of CuS-BSA-$Cu_3(PO_4)_2$ nanoparticles.

The XRD pattern, illustrated in **Figure 1**, depicts the crystallographic nature of CuS-BSA-$Cu_3(PO_4)_2$. The diffractogram comprises crystalline peaks located at 27.9°, 29.6°, 32.1°, 33.1°, 48.3°, 50.2° and 56.9° corresponding to the crystal planes of (101), (102), (103), (006), (110), and (114) with d-spacing of 3.20, 3.01, 2.78, 2.70, 1.88, 1.81 Å, respectively, in agreement with literature data [41, 42].

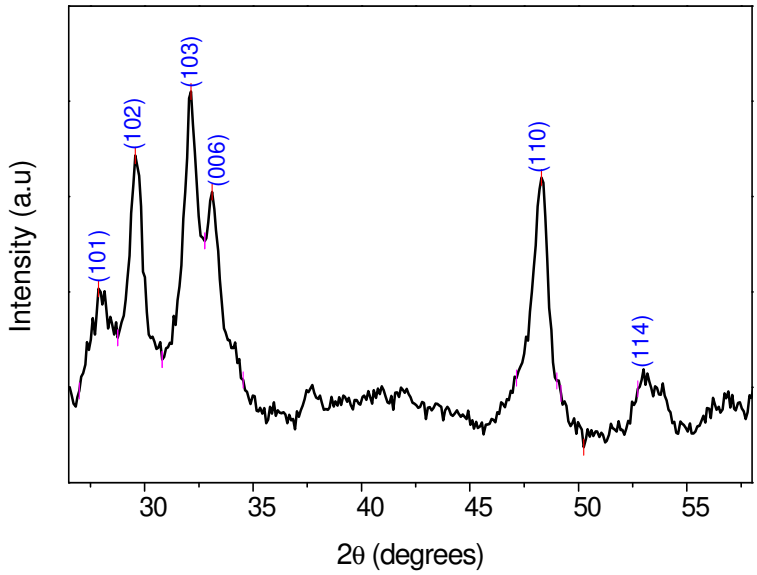

Figure 1: XRD pattern of CuS-BSA-$Cu_3(PO_4)_2$ nanoparticles.

To analyze the surface properties and the chemical composition of the prepared nanoparticles and to determine the chemical state of the Cu element in both CuS-BSA and CuS-BSA-$Cu_3(PO_4)_2$, X-ray photoelectron spectroscopy (XPS) analysis was performed. **Figure S5a** illustrates the XPS survey spectrum of CuS-BSA, where the peaks due to C_{1s} (284.6 eV), O_{1s} (531.8 eV), and N_{1s} (400.0 eV) of BSA molecules along with Cu_{2p} (932.0 eV) and S_{2p} (162.6 eV) due to CuS can be clearly observed, with atomic concentrations of 50.48, 30.23, 10.70, 6.75, and 1.84 at%, respectively. To get detailed information and inspect the various chemical groups, the high-resolution XPS spectrum of C in the 1s region **(Fig. S5b)** can be curve-fitted with several peaks at binding energies of 284.8, 285.8 and 287.8 eV, which are typical values for C-C/C-H, C-N/C-O, and C=O, respectively. The deconvolution of O_{1s} XPS spectrum **(Fig. S5c)** reveals the presence of O-H/C=O at 531.8 eV. The core level spectrum of the N_{1s} can be deconvoluted with two bands due to C-N and C=N at 399.8 and 402.2 eV, respectively. The high-resolution Cu_{2p} XPS spectrum is fitted with two peaks at binding energies of 934.2 and 954.1 eV assigned to $Cu_{2p3/2}$ and $Cu_{2p1/2}$,

respectively, along with two shake-up satellite features (**Fig. S5e**), confirming the presence of paramagnetic Cu^{2+} of CuS phase [43, 44]. The S_{2p} spectrum **(Fig. S5f)** encompasses two main peaks each deconvoluted with two bands ascribed to $S_{2p3/2}$ (162.6 eV), $S_{2p1/2}$ (163.8 eV) of CuS, and $S_{2p3/2}$ (167.1 eV), $S_{2p1/2}$ (168.8 eV) due to $CuSO_4$ which arises from the vulnerable oxidation of CuS [45].

After surface modification of CuS-BSA NPs with $Cu_3(PO_4)_2$, the XPS survey spectrum of CuS-BSA-$Cu_3(PO_4)_2$ nanoparticles exhibits in addition to the main peaks due to CuS and BSA, a peak assigned to P_{2p}, confirming the formation of CuS-BSA-$Cu_3(PO_4)_2$ NPs. **Figure S6a** depicts the XPS wide scan, comprising signals ascribed to the C_{1s} (~285 eV), O_{1s} (~531 eV), N_{1s} (~400 eV), Cu_{2p} (~932 eV), S_{2p} (~162 eV) and P_{2p} (~133 eV) with atomic concentrations of 62.69, 21.75, 12.91, 1.28, 0.59 and 0.75 at%, respectively. The C_{1s} high resolution spectrum with peak fitting is given in **Figure S6b**. It shows the existence of different components at 284.5 eV (C=C/C-C), 285.7 eV (C-N/C-O), and 287.7 eV (C=O) bonds. The O_{1s} core level spectrum can be curve-fitted with two separate components at 531.1 and 532.5 eV assigned to C=O/O-H and C-O/P-O, respectively **(Fig. S6c)**. The N_{1s} high resolution spectrum **(Fig. S6d)** can be deconvoluted into two bands at 399.6 and 401.8 eV related respectively to C-N and C=N bonds [25]. The Cu_{2p} high resolution spectrum **(Fig. S6e)** displays two peaks at 932.8 and 952.5eV corresponding respectively to $Cu_{2p3/2}$ and $Cu_{2p1/2}$ [46] separated by 19.7 eV [47], along with two "shakeup" satellite peaks located at 942.6 and 962.9 eV [48], which confirms the partially filled d-orbital of divalent copper (Cu^{2+}). It is worth to note that the binding energies of $Cu_{2p3/2}$ and $Cu_{2p1/2}$ are blue-shifted respectively by 1.4 and 1.6 eV, suggesting strong interaction of CuS and $Cu_3(PO_4)_2$. The deconvolution of the S_{2p} high resolution XPS spectrum indicates the presence of two main peaks corresponding to $S_{2p3/2}$ and $S_{2p1/2}$ at 161.7 and 162.9 eV, respectively due to sulfur element in S^{2-} state. The peaks at 167.8

and 169.0 eV are assigned respectively to $S_{2p3/2}$ and $S_{2p1/2}$ in S^{6+} oxidized state ($CuSO_4$) (**Fig. S5f**). The P_{2p} core level spectrum **(Fig. S6g)** comprises a single peak located at 133.18 eV ascribed to P-O bond in $Cu_3(PO_4)_2$ [49].

The surface morphology and structure of CuS-BSA-$Cu_3(PO_4)_2$ as well as their average size were examined by transmission electron microscopy (TEM) analysis. **Figure 2a** shows the TEM images of CuS-BSA-$Cu_3(PO_4)_2$ elucidating a relative agglomeration of the nanoparticles. A good crystal structure can be observed by high resolution TEM (HRTEM) and SAED pattern **(Fig. 2b)**, with a lattice fringe of 0.26 nm that correlates to the (006) crystal plane of CuS, in accordance with XRD analysis.

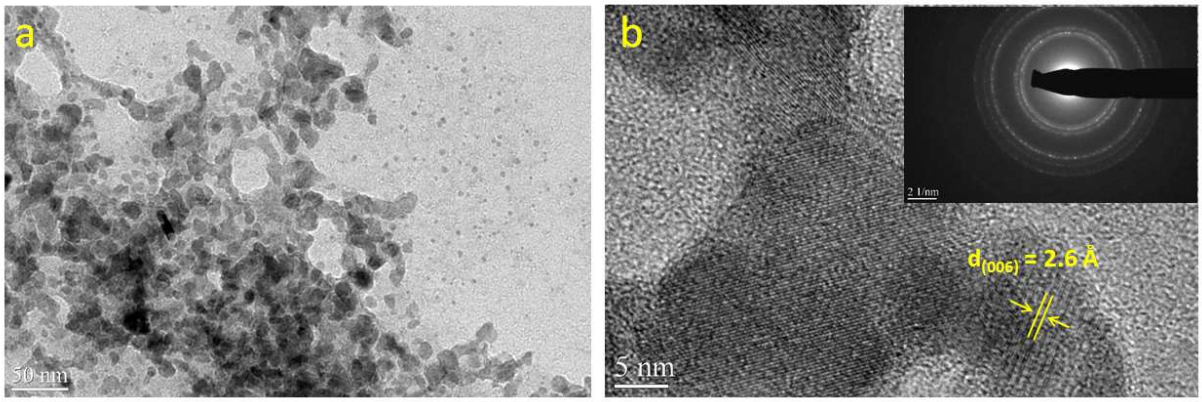

Figure 2: (a) TEM image, (b) high resolution TEM image and SAED pattern (inset b) of CuS-BSA-$Cu_3(PO_4)_2$ nanoparticles.

3.2. Enzyme-mimetic activity of CuS-BSA-$Cu_3(PO_4)_2$

The enzyme-mimetic activity of CuS-BSA-$Cu_3(PO_4)_2$ was evaluated for the catalytic oxidation of a chromogenic peroxidase substrate, 3,3',5,5'-tetramethylbenzidine (TMB), in presence of H_2O_2. In an acidic buffered medium, the proposed nanozyme successfully catalyzes the decomposition of H_2O_2 through a Fenton-mediated reaction [50] by the transition metal Cu^{2+} ion of the

synthesized nanoparticles to highly reactive hydroxyl radicals ($HO^{\bullet}$) that participate in the effective oxidation of TMB. The catalyzed reaction can be clearly recognized from a blue colored solution, corresponding to the oxidized product of TMB, "oxTMB", which exhibits an intense absorption maximum at 654 nm. The mechanism for $HO^{\bullet}$ generation can be summarized in the following equations (3,4) [31]:

$$Cu(II) + H_2O_2 \longrightarrow Cu(III) + HO^{\bullet} + HO^{-} \quad (3)$$

$$Cu(III) + H_2O_2 \longrightarrow Cu(II) + HOO^{\bullet} + H^{+} \quad (4)$$

On the basis of this assay, the enzyme-like catalytic reaction was carried out under different parameters to optimize the operating conditions and achieve the highest catalytic response.

To compare the effect of CuS-BSA-$Cu_3(PO_4)_2$ catalyst and H_2O_2 on TMB oxidation, we carried out control experiments in absence of H_2O_2 or CuS-BSA-$Cu_3(PO_4)_2$, and in presence of CuS-BSA-$Cu_3(PO_4)_2$ and H_2O_2 under the optimized reaction conditions. **Figure 3** shows that the highest catalytic activity was attained in presence of CuS-BSA-$Cu_3(PO_4)_2$ and H_2O_2, while TMB oxidation was not achieved when CuS-BSA-$Cu_3(PO_4)_2$ or H_2O_2 was absent. This indicates that both catalyst and H_2O_2 are required to obtain an enzyme-like catalytic reaction.

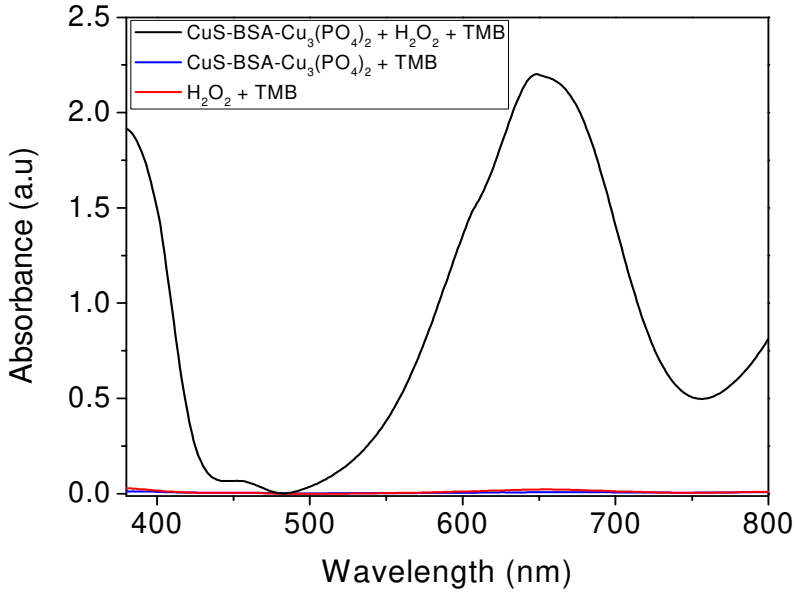

Figure 3: UV-Vis absorption spectra of oxTMB under different experimental conditions: 0.1 mg/mL CuS-BSA-$Cu_3(PO_4)_2$, 0.3 mM TMB, 1 mM H_2O_2, acetate buffer (0.1 M, pH 4), RT, 20 min incubation.

To optimize the experimental conditions for the enzyme-like catalyzed reaction, various parameters were tested. We first assessed the influence of different concentrations of CuS-BSA-$Cu_3(PO_4)_2$ (0-0.15 mg/mL), and TMB (0.01-0.35 mM) on the enzyme-like reaction. As depicted in **Figure S8**, the oxidation reaction of TMB is catalyst concentration-dependent, and saturates at 0.1 mg/mL of CuS-BSA-$Cu_3(PO_4)_2$. Thus, this concentration was adopted to initiate the subsequent experiments. At this value, TMB oxidation gives the highest absorption intensity at 0.3 mM, as clearly observed in **Figure S9**. Thereby, 0.3 mM of TMB was selected for the rest of the catalytic experiments.

The nanozyme-like catalyzed reaction can be also influenced by temperature, pH and time. Thus, the catalytic performance of CuS-BSA-$Cu_3(PO_4)_2$ was assessed at various temperatures between RT to 70°C **(Fig. S10a)**, and under a set of various pH values (3.6-10), **Fig. S10b**.

Interestingly, the nanozyme proved good catalytic action and this activity was not affected by temperature up to 40°C, under our experimental conditions. A continuous decrease of the nanozyme activity was evidenced for temperatures higher than 40°C, most likely due to H_2O_2 partial decomposition. Additionally, a slight acidic medium (pH 4) is required to achieve excellent catalytic behavior, as explained previously. Under these conditions, the reaction was completed within 20 min **(Fig. S11)**.

To gain a better insight about the influence of $Cu_3(PO_4)_2$ on the catalytic performance of the nanozyme, the oxidation of TMB was monitored in presence of CuS-BSA and $Cu_3(PO_4)_2$-BSA NPs. As can be seen in **Figure S12**, the activity of CuS-BSA-$Cu_3(PO_4)_2$ nanozyme is almost 3 and 2 times higher than that of CuS-BSA and $Cu_3(PO_4)_2$-BSA, respectively, indicating that $Cu_3(PO_4)_2$ enhances the catalytic properties of CuS-BSA due to the excess of Cu^{2+} ions on the catalyst surface.

Based on the obtained results, the kinetic study was conducted for determining the limit of H_2O_2 concentration needed to accomplish the catalytic reaction. Thereby, upon addition of various concentrations of H_2O_2 **(Fig. 4a and b)**, the maximum of absorption at 654 nm, which corresponds to the oxidized product of TMB, increases rapidly to reach a steady state at 1 mM. This was also confirmed by an intense color change **(inset of Fig. 4b)** achieved at this higher concentration of H_2O_2. A linear calibration curve for H_2O_2 within the 0 - 0.1 mM range was obtained, with a linear relation (R^2= 0.99815), and a detection limit of 0.16 µM was determined using **Eq. 1**.

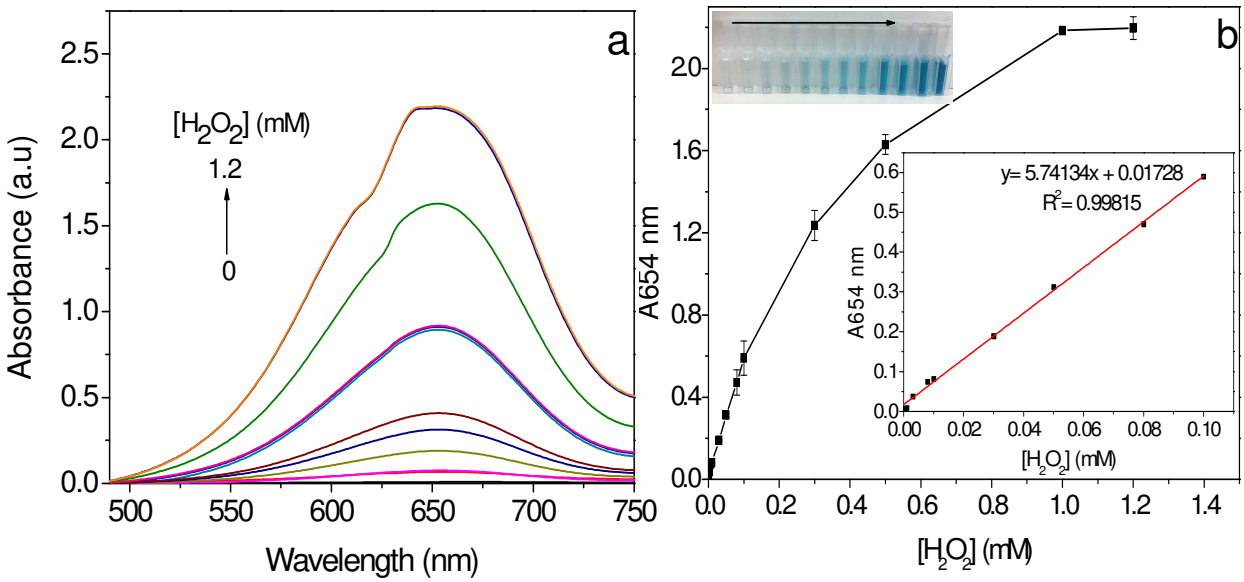

Figure 4: (a) UV-Vis absorbance spectra of oxTMB at different H_2O_2 concentrations, and (b) a dose-responsive curve of H_2O_2; reaction conditions: 0.3 mM TMB, 0.1 mg/mL CuS-BSA-$Cu_3(PO_4)_2$, acetate buffer (0.1 M, pH 4), RT, 20 min incubation. Inset (b): the linear calibration curve for H_2O_2 determination, and optical photographs of TMB oxidation at low (left) to high (right) H_2O_2 concentrations.

3.3. Michaelis-Menten kinetic assay of CuS-BSA-$Cu_3(PO_4)_2$

The steady state kinetics were studied using TMB and H_2O_2 as two different substrates at the optimal conditions, that is at 0.1 mg/mL CuS-BSA-$Cu_3(PO_4)_2$, pH 4, and RT. Thus, a set of catalytic experiments were executed by varying the concentration of one substrate while retaining the other constant, in a time-course mode, in order to assess the catalytic performance of the developed nanozyme. Beer-lambert law was used to estimate the initial rate of each substrate, which is calculated from the slope of absorbance at 654 nm per a unit time **(Eq.5)**.

$$A = \varepsilon \times C \times l \qquad (5)$$

Where A, C, ε, and l represent the oxTMB absorbance at 654 nm, concentration of the studied substrate, molar absorptivity of oxTMB (39000 $M^{-1}.cm^{-1}$), and the light path length (1 cm), respectively.

A plot of the initial catalytic reaction rate as a function of each substrate concentration is illustrated in **Figures S13a** and **S14a**, which also enables to draw a Lineweaver–Burk plot (**Fig. S13b** and **S14b)**, to calculate the kinetic parameters, where the slope determines the K_m and the intercept determines the V_{max} for TMB and H_2O_2. **Table 1** summarizes the kinetic parameters displayed by CuS-BSA-$Cu_3(PO_4)_2$ in comparison with reported literature. The K_m values for TMB and H_2O_2 exhibited by the proposed nanozyme were found to be lower than the natural horseradish peroxidase, elucidating a high affinity towards both substrates.

Table 1: Comparison of K_m and V_{max} kinetic parameters of H_2O_2 and TMB substrates with different reported sensing studies.

Catalyst	**K_m (mM)**		**V_{max} ($mM.s^{-1}$)**		**Ref.**
	H_2O_2	**TMB**	**H_2O_2**	**TMB**	
HRP	3.7	0.434	8.71×10^{-5}	10×10^{-5}	[51]
Ceria nanorods	293	0.417	3.8×10^{-2}	6.2×10^{-2}	[52]
Magnetic NPs	2.05	5.7	6.08×10^{-3}	1.43×10^{-4}	[53]
CuS-BSA-$Cu_3(PO_4)_2$	0.29	0.33	8.31×10^{-5}	1.6×10^{-4}	**This work**

3.4. Hydroxyl radicals' generation mechanism

It is well known that enzyme-like nanomaterials, mainly peroxidase mimics, have the ability to produce reactive oxygen species (ROS) such as hydroxyl radicals ($HO^{\bullet}$), which play a key role in the enzyme-like catalyzed reactions. Thus, to demonstrate $HO^{\bullet}$ generation during TMB oxidation, terephthalic acid (TA) was chosen as a probe analyte. TA was characterized by its capability to react with the generated $HO^{\bullet}$ in an acidic medium to yield a fluorescent product commonly named 2-hydroxyterephthalic acid (HTA), which can be easily monitored by fluorescent spectroscopy through an emission at 410 nm. Similarly, to emphasize that the existence of dopamine causes a decrease in the amount of $HO^{\bullet}$ radicals, fluorescence emission was also recorded in the presence of dopamine.

Figure S15 reveals that TA alone was not fluorescent. However, the simultaneous presence of CuS-BSA-$Cu_3(PO_4)_2$ and H_2O_2 in the reaction mixture greatly enhanced TA oxidation and resulted in an emission peak with a maximum at 410 nm. In contrast, upon addition of dopamine in the reaction mixture, the amount of the generated hydroxyl radicals is depleted, as evidenced by an immense reduction in the fluorescence intensity. This indicates that CuS-BSA-$Cu_3(PO_4)_2$ is a promising peroxidase mimetic and TMB oxidation in presence of H_2O_2 proceeds *via* the generation of $HO^{\bullet}$ radicals.

Furthermore, to gain more insight on $HO^{\bullet}$ formation during the catalytic process, the oxidation of TMB was performed in the presence of ROS scavenger, such as *t*-butyl alcohol (TBA), which is readily known to quench $HO^{\bullet}$ radicals. **Figure S16** depicts the variation of the maximum absorption intensity at 654 nm upon addition of 0.4 mM of TBA to a mixture of CuS-BSA-$Cu_3(PO_4)_2$ (0.1 mg/mL), H_2O_2 (1 mM) and TMB (0.3 mM) in acetate buffer (0.1 M, pH 4) for 20 min at RT. It is clearly observed that TBA lowers the rate of the enzyme-mimetic action of CuS-

BSA-$Cu_3(PO_4)_2$ nanoparticles by nearly 5 times, indicating that $HO^{\bullet}$ radicals are the main reactive species for TMB oxidation.

3.5. Nanozyme-mediated colorimetric determination of dopamine (DA)

Considering the enzyme-mimetic property of CuS-BSA-$Cu_3(PO_4)_2$ at the optimized conditions, a colorimetric sensor was designed for dopamine (DA) sensing. **Figure 5** depicts the DA concentration effect on the catalytic behavior of CuS-BSA-$Cu_3(PO_4)_2$ nanoparticles.

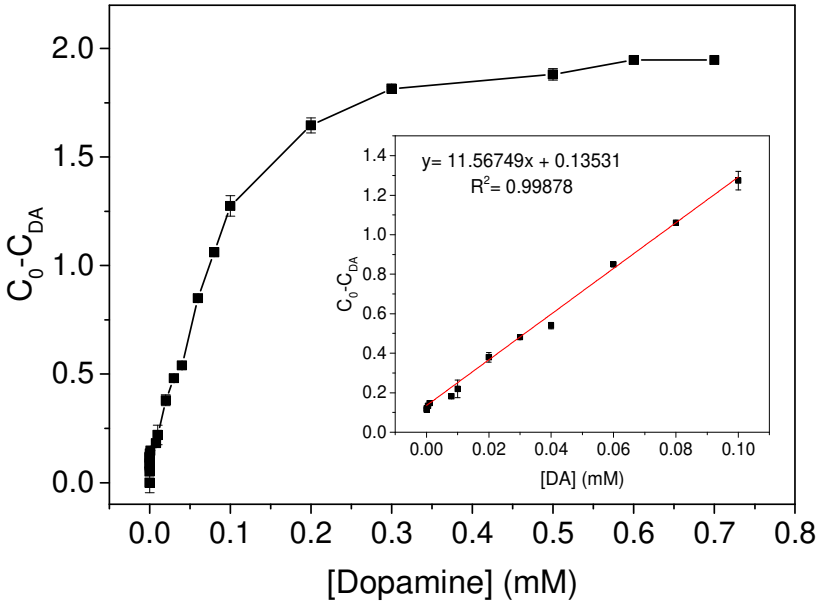

Figure 5: A dose responsive curve of oxTMB at different DA concentrations. Inset: linear calibration curve for DA determination and typical photographs of oxTMB at increasing concentrations of DA; reaction conditions: 0.3 mM TMB, 0.1 mg/mL CuS-BSA-$Cu_3(PO_4)_2$, 1 mM H_2O_2, acetate buffer (0.1 M, pH 4), RT, 20 min incubation.

Noticeably, the absorption intensity at 654 nm gradually decreases upon successive addition of DA, and a huge decline can be observed at an elevated amount of DA (0.5 mM), causing the blue oxTMB product to fade. This indicates that dopamine induces an inhibitory action of the

Fenton mediated reaction catalyzed by Cu(II) divalent ions of CuS-BSA-$Cu_3(PO_4)_2$ nanozyme as a result of $HO^{\bullet}$ quenching by DA, which results in the depletion of available $HO^{\bullet}$ in solution [22, 54]. DA sensing displays a linear equation y= -11.5675x (mM) + 0.1353 with a good linear relation (R^2= 0.9988) in the 0.05-0.1 mM concentration range **(inset of Fig. 5)** with a LOD as low as 0.13 µM, which has not achieved to date by colorimetric assays based on nanozymes. **Table 2** summarizes the LOD of DA obtained by various nanomaterials using colorimetric approaches, where CuS-BSA-$Cu_3(PO_4)_2$ displayed the highest sensitivity among all.

Table 2: Comparison of different colorimetric methods for dopamine sensing.

Sensor	**Incubation time (min)**	**Reaction temperature (°C)**	**Reaction pH**	**Linear range (µM)**	**LOD (µM)**	**References**
MOFs	30	45	4.0	0.05-30	0.50	[3]
GNPs	30	25	6.0	0.5-10	0.20	[20]
$NiCo_2S_4$-rGO	35	25	4.0	0.5-100	0.42	[21]
Pt-decorated Boron Nitride	20	35	4.0	2-50	0.76	[55]
CuS-rGO	15	30	4.4	2-100	0.48	[24]
CuS-BSA-$Cu_3(PO_4)_2$	20	25	4.0	0.05-100	0.13	**Present work**

3.6. CuS-BSA-$Cu_3(PO_4)_2$ nanozyme recyclability and selectivity

The reusability of the nanozyme was examined for 4 successive catalytic cycles. Before each repeated cycle, the CuS-BSA-$Cu_3(PO_4)_2$ nanosensor was separated by centrifugation and rinsed with Milli-Q water, followed by adding fresh solutions of TMB and H_2O_2 in acetate buffer to initiate the redox reaction. **Figure S17** indicates that the absorption intensity of oxTMB (654 nm) was slightly reduced after every cycle, which could be ascribed to the washing steps that causes loss of some amount of the catalyst.

Furthermore, the nanozyme selectivity towards dopamine sensing was evaluated in the presence of diverse biological molecules, and their absorption intensity at 654 nm was compared with that of DA. **Figure 6** indicates that interferences even at 0.6 mM (a concentration 2-times higher than DA) showed a very low reduction of the absorbance at 654 nm, which indicates good selectivity towards DA.

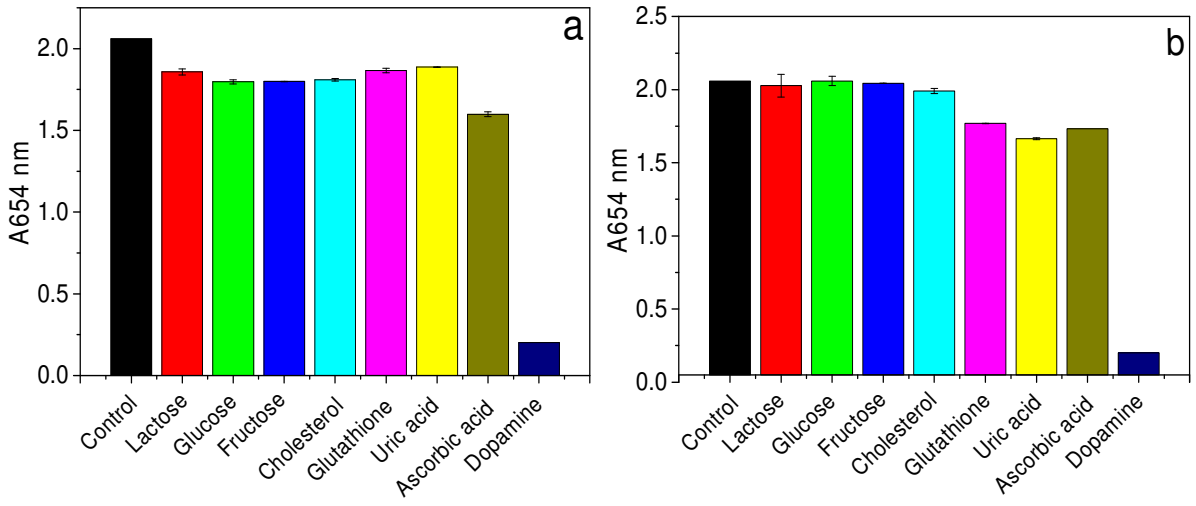

Figure 6: Comparison of oxTMB absorption in presence of different interfering molecules at a concentration of 0.3 mM (a) (same as DA) and 0.6 mM (b) (2 times higher than the concentration of DA); reaction conditions: 0.1 mg/mL CuS-BSA-$Cu_3(PO_4)_2$, 1 mM H_2O_2, 0.3 mM TMB, acetate buffer (0.1 M, pH 4), RT, 20 min incubation.

The inhibited oxidation of TMB in presence of DA is attributed to the addition of hydroxyl radicals on the phenolic ring of DA [1].

3.7. Sensing of DA in beef meat and blood samples

To evaluate the sensing performance of CuS-BSA-$Cu_3(PO_4)_2$ in real samples, we widen the scope of our investigation towards dopamine sensing in beef meat and serum samples. By comparing the oxTMB absorbance intensity at 654 nm, using the calibration curve in **Figure 5**, a DA concentration of 0.43 µM was determined in the diluted beef meat sample. HPLC analysis of meat samples was used to validate the results, which resulted in DA concentration of 0.4 µM using the calibration plot in **Figure S18**, in agreement with the colorimetric results.

Table 3: UV-vis and HPLC determination of dopamine in beef meat samples.

Sample	**Colorimetry**		**HPLC**	
	Absorbance (a.u)	[DA] (µM)	Peak area	[DA] (µM)
Beef meat	1.955	0.43	1386	0.4

DA sensing was also examined in blood samples spiked with different DA concentrations using the aforementioned optimized conditions. The DA concentration present in blood samples was determined from a previously established calibration plot at 654 nm using a set of DA concentrations. Relative standard deviation (RSD %) and percentage recovery ($[DA]_{found}/[DA)]_{added} \times 100$) in human serum samples are listed in **Table 4** (n=3), where the CuS-BSA-$Cu_3(PO_4)_2$ nanozyme exhibited good recovery percentage for dopamine detection in human serum samples.

Table 4: Sensing DA in human serum samples (n=3).

Samples	DA added (µM)	DA found (µM)	RSD (%)	Recovery (%)
Human blood sample	5.0	5.8	2.7	116.4
	10.0	8.8	2.2	87.9
	15.0	17.5	2.8	116.8
	50.0	49.4	7.3	98.8

4. Conclusion

Sensitive and accurate dopamine (DA) sensing represents an indispensable need to achieve early disease diagnosis and therapeutic purposes as well as to prevent illegal use of DA in animal feed. Commonly, DA sensing was achieved using electrochemical means, while colorimetric detection was only reported in a few reports. In this work, we used engineered CuS-BSA-$Cu_3(PO_4)_2$ nanoparticles with high stability, dispersibility and enhanced catalytic activity as a promising platform for colorimetric sensing assays. The designed CuS-BSA-$Cu_3(PO_4)_2$ nanosensor exhibited a peroxidase-like action through TMB oxidation in presence of H_2O_2 to give a blue-colored (oxTMB) product, due to their huge efficacy in generating reactive oxygen species (ROS) such as hydroxyl radicals ($HO^{\bullet}$). This phenomenon showed to be impeded in the presence of dopamine, which was then successfully applied for dopamine sensing with high sensitivity and good selectivity. The obtained results proved that the proposed colorimetric sensor achieved a simple, rapid, and sensitive quantification of dopamine and provides a feasible low-cost analysis method. The good sensitivity (LOD=0.13 µM) of the developed nanosensor, which is better than that achieved in the literature, allowed testing its robustness in meat and blood samples. Future

work using emerging paper-based analytical devices will open new opportunities for designing simple, inexpensive and rapid sensing systems required for a myriad of uses.

References

[1] G.-C. Yen, C.-L. Hsieh, Antioxidant effects of dopamine and related compounds, Biosci. Biotechnol. Biochem. 61 (1997) 1646-1649.

[2] J. Liu, L. Yuan, X. Dong, Recent advances in analytical techniques for the determination of dopamine, Int. J. Chem. Stud. 3 (2015) 39-45.

[3] C. Zhao, Y. Liu, Y. Li, Colorimetric and Fluorometric Assays for Dopamine with a Wide Concentration Range Based on Fe-MIL-88NH_2 Metal-organic Framework, Anal. Sci. 31 (2015) 1035-1039.

[4] Y. Tao, Y. Lin, J. Ren, X. Qu, A dual fluorometric and colorimetric sensor for dopamine based on BSA-stabilized Aunanoclusters, Biosens. Bioelectron. 42 (2013) 41-46.

[5] L. Zhihua, Z. Xucheng, W. Kun, Z. Xiaobo, S. Jiyong, H. Xiaowei, et al., A novel sensor for determination of dopamine in meat based on ZnO-decorated reduced graphene oxide composites, Innovative Food Sci. Emerg. Technol. 31 (2015) 196-203.

[6] H.-X. Zhao, H. Mu, Y.-H. Bai, H. Yu, Y.-M. Hu, A rapid method for the determination of dopamine in porcine muscle by pre-column derivatization and HPLC with fluorescence detection, J. Pharm. Anal. 1 (2011) 208-212.

[7] G.E. De Benedetto, D. Fico, A. Pennetta, C. Malitesta, G. Nicolardi, D.D. Lofrumento, et al., A rapid and simple method for the determination of 3,4-dihydroxyphenylacetic acid,

norepinephrine, dopamine, and serotonin in mouse brain homogenate by HPLC with fluorimetric detection, J. Pharm. Biomed. Anal. 98 (2014) 266-270.

[8] X. Wang, Y. Ma, X. Yao, J. Wang, M. Yin, Determination of dopamine in rat less differentiated pheochromocytoma cells by capillary electrophoresis with a palladium nanoparticles microdisk electrode, RSC Adv. 3 (2013) 24605-24611.

[9] R. Cui, Y.-P. Gu, L. Bao, J.-Y. Zhao, B.-P. Qi, Z.-L. Zhang, et al., Near-infrared electrogenerated chemiluminescence of ultrasmall Ag2Se quantum dots for the detection of dopamine, Anal. Chem. 84 (2012) 8932-8935.

[10] H. Fang, M.L. Pajski, A.E. Ross, B.J. Venton, Quantitation of dopamine, serotonin and adenosine content in a tissue punch from a brain slice using capillary electrophoresis with fast-scan cyclic voltammetry detection, Anal. Methods 5 (2013) 2704-2711.

[11] Y. Zhou, M. He, C. Huang, S. Dong, J. Zheng, A novel and simple biosensor based on poly (indoleacetic acid) film and its application for simultaneous electrochemical determination of dopamine and epinephrine in the presence of ascorbic acid, J. Solid-State Electrochem. 16 (2012) 2203-2210.

[12] B. Li, Y. Zhou, W. Wu, M. Liu, S. Mei, Y. Zhou, et al., Highly selective and sensitive determination of dopamine by the novel molecularly imprinted poly (nicotinamide)/CuO nanoparticles modified electrode, Biosens. Bioelectron. 67 (2015) 121-128.

[13] Y.-R. Kim, S. Bong, Y.-J. Kang, Y. Yang, R.K. Mahajan, J.S. Kim, et al., Electrochemical detection of dopamine in the presence of ascorbic acid using graphene modified electrodes, Biosens. Bioelectron. 25 (2010) 2366-2369.

[14] A. Hermans, Fabrication and applications of dopamine-sensitive electrodes: The University of North Carolina at Chapel Hill; 2007.

[15] G.-C. Yen, P.-D. Duh, H.-L. Tsai, Antioxidant and pro-oxidant properties of ascorbic acid and gallic acid, Food Chem. 79 (2002) 307-313.

[16] J. Yang, J.R. Strickler, S. Gunasekaran, Indium tin oxide-coated glass modified with reduced graphene oxide sheets and gold nanoparticles as disposable working electrodes for dopamine sensing in meat samples, Nanoscale 4 (2012) 4594-4602.

[17] M.N. Karim, M. Singh, P. Weerathunge, P. Bian, R. Zheng, C. Dekiwadia, et al., Visible-light-triggered reactive-oxygen-species-mediated antibacterial activity of peroxidase-mimic CuO nanorods, ACS Appl. Nano Mater. 1 (2018) 1694-1704.

[18] Y. Lin, J. Ren, X. Qu, Catalytically active nanomaterials: a promising candidate for artificial enzymes, Acc. Chem. Res. 47 (2014) 1097-1105.

[19] X. Wang, Y. Hu, H. Wei, Nanozymes in bionanotechnology: from sensing to therapeutics and beyond, Inorg. Chem. Front. 3 (2016) 41-60.

[20] H. Su, B. Sun, L. Chen, Z. Xu, S. Ai, Colorimetric sensing of dopamine based on the aggregation of gold nanoparticles induced by copper ions, Anal. Methods 4 (2012) 3981-3986.

[21] Y. Wang, L. Yang, Y. Liu, Q. Zhao, F. Ding, P. Zou, et al., Colorimetric determination of dopamine by exploiting the enhanced oxidase mimicking activity of hierarchical $NiCo_2S_4$-rGO composites, Microchim. Acta 185 (2018) 496.

[22] M. Ivanova, E.D. Grayfer, E.E. Plotnikova, L.S. Kibis, G. Darabdhara, P.K. Boruah, et al., Pt-Decorated Boron Nitride Nanosheets as Artificial Nanozymes for Detection of Dopamine, ACS Appl. Mater. Interfaces (2019).

[23] J.-J. Feng, H. Guo, Y.-F. Li, Y.-H. Wang, W.-Y. Chen, A.-J. Wang, Single molecular functionalized gold nanoparticles for hydrogen-bonding recognition and colorimetric detection of dopamine with high sensitivity and selectivity, ACS Appl. Mater. Interfaces 5 (2013) 1226-1231.

[24] S. Dutta, C. Ray, S. Mallick, S. Sarkar, R. Sahoo, Y. Negishi, et al., A gel-based approach to design hierarchical CuS decorated reduced graphene oxide nanosheets for enhanced peroxidase-like activity leading to colorimetric detection of dopamine, J. Phys. Chem. C 119 (2015) 23790-23800.

[25] J. Gao, H. Liu, L. Pang, K. Guo, J. Li, Biocatalyst and Colorimetric/Fluorescent Dual Biosensors of H_2O_2 Constructed via Hemoglobin–$Cu_3(PO_4)_2$ Organic/Inorganic Hybrid Nanoflowers, ACS Appl. Mater. Interfaces 10 (2018) 30441-30450.

[26] C. Wang, J. Gao, Y. Cao, H. Tan, Colorimetric logic gate for alkaline phosphatase based on copper (II)-based metal-organic frameworks with peroxidase-like activity, Anal. Chim. Acta 1004 (2018) 74-81.

[27] Q. Wu, L. He, Z.W. Jiang, Y. Li, Z.M. Cao, C.Z. Huang, et al., CuO nanoparticles derived from metal-organic gel with excellent electrocatalytic and peroxidase-mimicking activities for glucose and cholesterol detection, Biosens. Bioelectron. (2019) 111704.

[28] A.P. Nagvenkar, A. Gedanken, $Cu_{0.89}Zn_{0.11}O$, a new peroxidase-mimicking nanozyme with high sensitivity for glucose and antioxidant detection, ACS Appl. Mater. Interfaces 8 (2016) 22301-22308.

[29] S. Goel, F. Chen, W. Cai, Synthesis and biomedical applications of copper sulfide nanoparticles: from sensors to theranostics, Small 10 (2014) 631-645.

[30] Y. Zhang, Y.-N. Wang, X.-T. Sun, L. Chen, Z.-R. Xu, Boron nitride nanosheet/CuS nanocomposites as mimetic peroxidase for sensitive colorimetric detection of cholesterol, Sens. Actuators B 246 (2017) 118-126.

[31] A. Swaidan, P. Borthakur, P.K. Boruah, M.R. Das, A. Barras, S. Hamieh, et al., A facile preparation of CuS-BSA nanocomposite as enzyme mimics: Application for selective and sensitive sensing of Cr (VI) ions, Sens. Actuators B 294 (2019) 253-262.

[32] A.K. Dutta, S. Das, S. Samanta, P.K. Samanta, B. Adhikary, P. Biswas, CuS nanoparticles as a mimic peroxidase for colorimetric estimation of human blood glucose level, Talanta 107 (2013) 361-367.

[33] W. Xue, T. Cheng-Ling, L. Jia-Jun, H.-Z. ZHANG, W. Jian, Ultra-small CuS nanoparticles as peroxidase mimetics for sensitive and colorimetric detection of uric acid in human serum, Chin. J. Anal. Chem. 46 (2018) e1825-e1831.

[34] X. Niu, Y. He, J. Pan, X. Li, F. Qiu, Y. Yan, et al., Uncapped nanobranch-based CuS clews used as an efficient peroxidase mimic enable the visual detection of hydrogen peroxide and glucose with fast response, Anal. Chim. Acta 947 (2016) 42-49.

[35] H. Wei, E. Wang, Nanomaterials with enzyme-like characteristics (nanozymes): next-generation artificial enzymes, Chem. Soc. Rev. 42 (2013) 6060-6093.

[36] K. Kahlouche, R. Jijie, I. Hosu, A. Barras, T. Gharbi, R. Yahiaoui, et al., Controlled modification of electrochemical microsystems with polyethylenimine/reduced graphene oxide using electrophoretic deposition: Sensing of dopamine levels in meat samples, Talanta 178 (2018) 432-440.

[37] X. Yu, C. Qian, X. Wang, Microbiological precipitation, morphology and thermal behavior of barium hydrogen phosphate, J. Chil. Chem. Soc. 60 (2015) 2885-2887.

[38] L. Liang, X. Fei, Y. Li, J. Tian, L. Xu, X. Wang, et al., Hierarchical assembly of enzyme-inorganic composite materials with extremely high enzyme activity, RSC Adv. 5 (2015) 96997-97002.

[39] X. Wen, H. Zhang, Photoelectrochemical Properties of CuS-GeO_2-TiO_2 Composite Coating Electrode, PloS one 11 (2016) e0152862.

[40] J. Grdadolnik, Y. Maréchal, Bovine serum albumin observed by infrared spectrometry. I. Methodology, structural investigation, and water uptake, Biopolymers 62 (2001) 40-53.

[41] S. Riyaz, A. Parveen, A. Azam, Microstructural and optical properties of CuS nanoparticles prepared by sol–gel route, Perspect. Sci. 8 (2016) 632-635.

[42] M. Tanveer, C. Cao, Z. Ali, I. Aslam, F. Idrees, W.S. Khan, et al., Template free synthesis of CuS nanosheet-based hierarchical microspheres: an efficient natural light driven photocatalyst, CrystEngComm 16 (2014) 5290-5300.

[43] J. Yu, J. Zhang, S. Liu, Ion-exchange synthesis and enhanced visible-light photoactivity of CuS/ZnS nanocomposite hollow spheres, J. Phys. Chem. C 114 (2010) 13642-13649.

[44] J. Zhang, J. Yu, Y. Zhang, Q. Li, J.R. Gong, Visible light photocatalytic H2-production activity of CuS/ZnS porous nanosheets based on photoinduced interfacial charge transfer, Nano Lett. 11 (2011) 4774-4779.

[45] C.-J. Chang, Y.-H. Wei, W.-S. Kuo, Free-standing CuS–ZnS decorated carbon nanotube films as immobilized photocatalysts for hydrogen production, Int. J. Hydrogen Energy (2018).

[46] H. Yan, J. Chen, Y. Li, Y. Bai, Y. Wu, Z. Sheng, et al., Ultrasmall hybrid protein–copper sulfide nanoparticles for targeted photoacoustic imaging of orthotopic hepatocellular carcinoma with a high signal-to-noise ratio, Biomater. Sci. 7 (2019) 92-103.

[47] A.C. Poulose, S. Veeranarayanan, M.S. Mohamed, R.R. Aburto, T. Mitcham, R.R. Bouchard, et al., Multifunctional $Cu_{2-x}Te$ Nanocubes Mediated Combination Therapy for Multi-Drug Resistant MDA MB 453, Sci. Rep. 6 (2016) 35961.

[48] C. Ye, M.Q. Wang, L.J. Li, H.Q. Luo, N.B. Li, Fabrication of $Pt/Cu_3(PO_4)_2$ ultrathin nanosheet heterostructure for photoelectrochemical microRNA sensing using novel G-wire-enhanced strategy, Nanoscale 9 (2017) 7526-7532.

[49] S. Hu, Z. Chen, X. Guo, Inhibition Effect of Three-Dimensional (3D) Nanostructures on the Corrosion Resistance of 1-Dodecanethiol Self-Assembled Monolayer on Copper in NaCl Solution, Materials 11 (2018) 1225.

[50] B. Halliwell, J.M. Gutteridge, Free radicals in biology and medicine: Oxford University Press, USA; 2015.

[51] L. Gao, J. Zhuang, L. Nie, J. Zhang, Y. Zhang, N. Gu, et al., Intrinsic peroxidase-like activity of ferromagnetic nanoparticles, Nature Nanotechnol. 2 (2007) 577.

[52] Z. Tian, J. Li, Z. Zhang, W. Gao, X. Zhou, Y. Qu, Highly sensitive and robust peroxidase-like activity of porous nanorods of ceria and their application for breast cancer detection, Biomaterials 59 (2015) 116-124.

[53] S. Luo, Y. Liu, H. Rao, Y. Wang, X. Wang, Fluorescence and magnetic nanocomposite Fe_3O_4@SiO_2@Au MNPs as peroxidase mimetics for glucose detection, Anal. Biochem. 538 (2017) 26-33.

[54] A. Slivka, G. Cohen, Hydroxyl radical attack on dopamine, J. Biol. Chem. 260 (1985) 15466-15472.

[55] M. Ivanova, E.D. Grayfer, E.E. Plotnikova, L.S. Kibis, G. Darabdhara, P.K. Boruah, et al., Pt-Decorated Boron Nitride Nanosheets as Artificial Nanozymes for Detection of Dopamine, ACS Appl. Mater. Interfaces 11 (2019) 22102−22112.

Graphical Abstract